Optics and Lasers in Engineering 160 (2023) 107287

Contents lists available at ScienceDirect

Optics and Lasers in Engineering

journal homepage: www.elsevier.com/locate/optlaseng

On-ground demonstration of laser-link construction for space-based detection of gravitational waves

Ruihong Gao[a,b,c,e,1,*], Yikun Wang[d,e,f,1], Zhao Cui[d,e], Heshan Liu[c], Anwei Liu[f], Xingguang Qian[d,e], Xue Wang[f], Zhixiong Yao[g], Qiujie Yang[f], Jianjun Jia[b,d,e,f], Keqi Qi[c], Shaoxin Wang[c], Ziren Luo[c,*], Gang Jin[a,*], Jianyu Wang[d,e,f,*]

[a] School of Fundamental Physics and Mathematical Sciences, Hangzhou Institute for Advanced Study, UCAS, Hangzhou, 310024, China
[b] University of Chinese Academy of Sciences, Beijing, 100049, China
[c] Institute of Mechanics, Chinese Academy of Sciences, Beijing, 100190, China
[d] School of Physics and Optoelectronic Engineering, Hangzhou Institute for Advanced Study, UCAS, Hangzhou, 310024, China
[e] Key Laboratory of Gravitational Wave Precision Measurement of Zhejiang Province, Hangzhou Institute for Advanced Study, UCAS, Hangzhou,310024, China
[f] Key Laboratory of Space Active Opto-Electronics Technology, Shanghai Institute of Technical Physics, Chinese Academy of Sciences, Shanghai,200083, China
[g] Zhejiang Lab, Hangzhou,311121, China

ARTICLE INFO

Keywords:
Gravitational wave detection
Interferometer
Laser acquisition
Differential wavefront sensing
Experimental demonstration system

ABSTRACT

Laser acquisition and pointing system is subject to establish a 10^6 km magnitude inter-satellite laser link with ultra-high pointing precision of 10 nrad/$\sqrt{\text{Hz}}$ (1 mHz-1 Hz) in space-based gravitational wave detection missions. For the unprecedented challenge, a dedicated laser link construction scheme with three different detectors is proposed. After initial pointing with star trackers, CMOS/CCD cameras intend to suppress the laser pointing error to 1 μrad. QPDs are subsequently used to achieve the final requirement. With various detectors and technologies, the scheme need intensive verification and study. We first design and build an on-ground laser link construction experimental system, which can simulate the whole process and recreate the actual critical working condition as realistic as possible by comprehensively considering the simulation of optical system, far field beam receiving characteristics and target precision. Results are well in agreement with the requirements and confirm the scheme under realistic conditions, which have not yet been fully tested experimentally.

1. Introduction

Laser acquisition and pointing technique plays a vital role in inter-satellite laser communication and precision measurement areas for constructing a stable laser link. With different payloads and targets, various acquisition schemes have been proposed [15,18,21,23,24]. It is now well established from a variety of studies and missions, that an inter-satellite laser link of 10^5 km magnitude can be constructed with the laser pointing error of 1 μrad magnitude [14]. However, difficulty in technical realization greatly increases with the increase of acquisition distance and pointing precision. In space-based gravitational wave detection missions, such as the LISA (Laser Interferometer Space Antenna) [13] and the Taiji program [16], an equilateral triangle laser link, whose arm length is as long as 10^6 km scale, has to be established before science measurement. On the other hand, the laser pointing jitter need to be suppressed to 10 nrad/$\sqrt{\text{Hz}}$ (1 mHz-1 Hz) for achieving arm-length variations measurement of picometer precision [12,13]. Because of the ultra-far acquisition distance, ultra-high pointing precision requirement and restricted payload for laser link construction, traditional laser acquisition and pointing schemes are not applicable. Thus, a dedicated laser link construction scheme with three different detectors is proposed for the LISA-like missions [1,5,11,17].

It stands to reason that, after one laser link is performed on one arm, the signal acquisition process on the second and third arm will be in principle the same. Thus, the signal acquisition of the single arm is most concerned. The whole process can be divided into laser acquisition phase and laser pointing phase. (1) Firstly, STRs (Star Trackers) are used to preliminarily suppress the laser pointing error. After initial pointing, the remote satellite is sited within an uncertainty cone of approximate 20 μrad [6]. (2) Then, in the laser acquisition phase, CCD/CMOS acquisition cameras with smaller FOV (Field of View) and higher sensitivity are used to further suppress the laser pointing error. The two satellites on each end of the link are defined as SC1 and SC2. At the beginning, SC1 keeps staring into its reference direction, while SC2 performs a scanning

* Corresponding authors.
E-mail addresses: gaoruihong@ucas.ac.cn (R. Gao), luoziren@imech.ac.cn (Z. Luo), gajin@imech.ac.cn (G. Jin), jywang@mail.sitp.ac.cn (J. Wang).
[1] These two authors contributed equally.

https://doi.org/10.1016/j.optlaseng.2022.107287
Received 25 January 2022; Received in revised form 19 August 2022; Accepted 12 September 2022
Available online 24 September 2022

maneuver to cover the whole uncertainty cone of SC1. At a certain time, laser signal with enough power can be received by SC1 and imaged on the acquisition camera with the help of a dedicated imaging system. After measuring the offset between the laser spot center position and the reference position, SC1 can adjust its line of sight and point to the direction of SC2. As a result, SC2 will also receive the transmitting laser beam. With the same method, the direction of SC2 can also be adjusted. Once both satellites have successfully received a laser signal on their acquisition cameras, a fine attitude closed-loop control can be performed based on the read-out of the cameras. The laser pointing error is intended to be suppressed to 1 μrad after acquisition process, which is much smaller than the FOV of the QPD (Quadrant Photodiode). As a result, the QPDs can receive interference signal continuously after laser frequency scan [1]. (3) Finally, QPDs are used in the laser pointing phase. With the help of the DWS (Differential Wavefront Sensing) technique [9,19,20], the included angle of the interference laser beams can be readout accurately based on the measurement of phase difference between up and down (or right and left) quadrants of QPDs. Through feedback control, the laser pointing jitter can be kept at 10 $\mathrm{nrad}/\sqrt{\mathrm{Hz}}$.

The above laser link construction scheme includes various detectors and measuring techniques for achieving the ultra-high accuracy requirement. Thus, a considerable amount of literature has been published on the laser link construction system of the LISA/Taiji to demonstrate the feasibility of the extremely challenging scheme. The acquisition scheme has been verified with simulation method [11,17], while the acquisition controller has been well designed based on a Kalman filter [1,2]. In the studies on the laser pointing phase, the relative importance of the DWS technique has been subject to considerable discussion. Theoretical derivation and simulation results presented the potential of the DWS for reaching the angular measurement precision of 1 $\mathrm{nrad}/\sqrt{\mathrm{Hz}}$ magnitude [4,9]. Principle methodology demonstration experiments of laser pointing system further proved its feasibility [3,8]. However, few writers have been able to draw on any systematic research into the whole laser link construction process from the perspective of simulation experiment or engineering implementation. Although the whole process is divided into laser acquisition phase and laser pointing phase, their optical system and system parameters are strongly coupled. Moreover, compared with theoretical analysis and simulation method, a well designed experimental system can help us expose, resolve and validate technique problems. As a result, a laser link construction on-ground simulation experiment, including laser acquisition and laser pointing process, will play a decisive role in demonstration of the proposed scheme. This paper first focuses on the design and construction of the on-ground experimental system. We present an experiment that simulates the optical system, process, far field beam receiving characteristics and target accuracy of the actual Taiji laser link construction system, making it an fully demonstration on the relevant core measurement techniques and the whole scheme.

The essay has been organised in the following way. In section 2, details of the experimental system design is presented including optical design and system parameter design. The section 3 is concerned with the construction and implementation of the experiment. The experiment results are shown and discussed in section 4, followed by a summary in section 5.

2. System Design

The objective of our on-ground experiment is to simulate the actual laser link construction system for gravitational wave detection missions as realist as possible and achieve the target precision requirements of laser acquisition & pointing at the same time. Make the Taiji program as an example, each satellite has an identical optical platform, containing all the elements of the laser link construction system. After emitting from the laser, the beam firstly reflect by a PAAM (Point Ahead Angle Mechanism) [10], which compensates the point ahead angle caused by satellite lateral motion. Then, the laser beam passes through a telescope and transmits to the remote satellite. The laser link construction system of Taiji is a transmitting-receiving common path system. Thus, the receiving laser beam passes through the same telescope. Then it is divided into two beams and respectively transmit to acquisition cameras and QPDs. In the acquisition phase, the attitude of the satellite is adjusted based on the readout signal of the cameras. After the receiving beam entering the FOV of the QPDs, the DWS signal is served to fine adjust the line of sight.

Table 1
Core system parameters of the Taiji program and the laser link construction on-ground experiment.Where, L is the platform separation, ω_0 is the beam waist radius, α is the half angle of scanning range, R_{uc} is the radius of the uncertainty cone, ω_z is the beam radius at the receiving aperture, ε is the aperture radius, m_{flat} is the flat top beam approximate coefficient, n_{scan} is the scanning range coefficient, P_{rec} is the laser power at the receiving aperture, P_{CMOS} is the laser power at the CMOS camera, P_{QPD} is the receiving laser power at the QPD, P_{local} is the local laser power at the QPD, f_{beat} is the beat frequency of the interference signal, $\phi_{acq,tel}$ is the target acquisition precision at the telescope, $\phi_{acq,CMOS}$ is the target acquisition precision at the CMOS, $\phi_{point,tel}$ is the target laser pointing precision at the telescope and $\phi_{point,QPD}$ is the target laser pointing precision at the QPD.

Parameter	Taiji program	Experiment
L	3×10^6 km	10 m
ω_0	20 cm	0.5 mm
α	24 μrad	700 μrad
R_{uc}	72 km	7 mm
ω_z	5 km	6.5 mm
ε	20 cm	0.5 mm
m_{flat}	2.5×10^4	13
n_{scan}	14.4	1.1
P_{rec}	1.5 nW	~1 μW
P_{CMOS}	~100 pW	~100 pW
P_{QPD}	~1 nW	~100 nW
P_{loc}	~10 μW	~10 μ
f_{beat}	1 ~ 20 MHz	2 MHz
$\phi_{acq,tel}$	1 μrad	/
$\phi_{acq,QPD}$	400 μrad	400 μrad
$\phi_{point,tel}$	10 $\mathrm{nrad}/\sqrt{\mathrm{Hz}}$	/
$\phi_{point,QPD}$	4 $\mu\mathrm{rad}/\sqrt{\mathrm{Hz}}$	4 $\mu\mathrm{rad}/\sqrt{\mathrm{Hz}}$

2.1. Optical design

In the experiment, the optical system aims at restoring the above functions. As shown in Fig. 1, two identical optical benches are respectively mounted on two hexapods, with the separation distance of about 10 m. PI P-915K652 hexapods, whose minimum angular incremental motion is as small as 70 nrad, are used to simulate the motion of the satellites. Because of restricted beam transmission distance on ground, the telescopes are replaced by small apertures for simulating far field beam receiving characteristics (details are introduced in section 2.2). As a result, the influence of wavefront distortion caused by the telescope is ignored. However, based on previous research, a well designed telescope, whose wavefront distortion is kept within $\lambda/30$, will have little impact on acquisition system [25]. From Fig. 1, it can be seen that the transmitting beam passes through the aperture center to the opposite platform. After clipped by the opposite aperture, the receiving laser is divided into two beams and transmits to the CMOS camera and the QPDs respectively. The aperture is centrally located on the optical bench, near the rotation center of the hexapod. The advantage is that the rotation of the hexapod will induce minor unwanted change of the entrance pupil position. The PAAM system is replaced by a mirror, as no extra platform lateral motion will be introduced. A dedicated imaging system is designed, making the aperture surface and the QPD surface compose a conjugate plane pair. It can greatly reduce the influence of beam walk to interference efficiency and DWS linearity performance. The CMOS receives Airy spots of 100-picowatt magnitude with the help of an imaging lens and a neutral density filter.

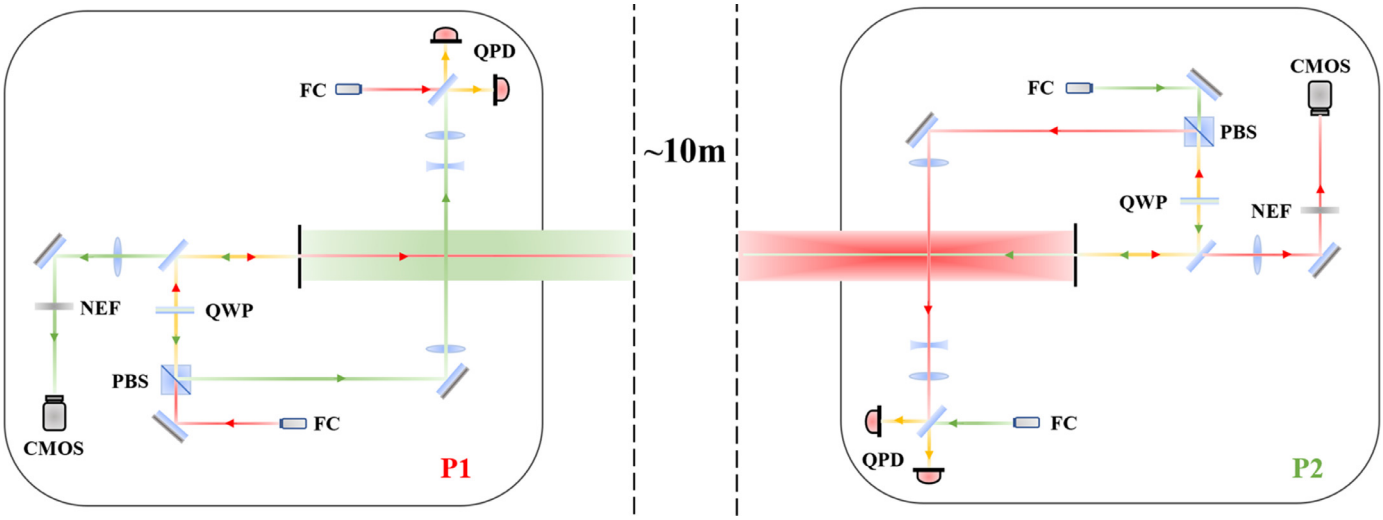

Fig. 1. Diagram of the laser link construction on-ground experiment system. Where, FC is fiber collimator, PBS is polarized beam splitter, QWP is quarter wave plate and NEF is neutral density filter.

In the Taiji program, the acquisition precision of 1 μrad and the laser pointing precision of 10 $\text{nrad}/\sqrt{\text{Hz}}$ are required at the telescope. Besides that, the magnification of the telescope is 100× and the magnification of the imaging system before QPD is 4×. While the laser spot at the QPD is reduced 400 times by the whole optical system, the laser pointing angle is amplified 400 times at the same time. Correspondingly, the acquisition precision required at the QPD is 400 μrad, while the laser pointing precision is 4 $\mu\text{rad}/\sqrt{\text{Hz}}$. These requirements are equivalent for the measurement system. As there is no telescope in the experimental system, we estimate the laser pointing error at the QPDs. For examining the acquisition precision, the DWS signal read out by the QPD is used. Meanwhile, The laser pointing precision is evaluated by the ASD (Amplitude Spectral Density) of the DWS results. For achieving the requirements, the system parameter design is introduced in the next sub-section.

2.2. System parameter design

Except for optical system, far field beam receiving characteristics simulation need to be considered most. Table I presents the core system parameters of the Taiji program. Because of the extremely far beam transmitting distance, the beam radius at the receiving aperture ω_z is far larger than the aperture radius ε. Thus, the received beam has spherical wavefront feature as well as homogeneous intensity distribution, that is a flat top beam. Based on the spherical wavefront feature, the direction of the remote satellite can be uniquely determined without considering the relative position relationship between the receiving laser spot and the aperture. While only with homogeneous intensity distribution, can the laser spot center position be used for the determination of the line of sight offset. Therefore, the flat top beam simulation is one of the most important factor for guaranteeing effectiveness of the acquisition scheme. We define the flat top beam approximate coefficient m_{flat} as the ratio of ω_z and ε. After expansion, m_{flat} can be written as,

$$m_{flat} = \frac{\sqrt{\omega_0^2 + \frac{\lambda^2 L^2}{\pi^2 \omega_0^2}}}{\varepsilon}, \tag{1}$$

where, ω_0 is the beam waist radius and L is the platform separation. From formula (1) we can find that, m_{flat} increases with the increase of L. For the beam transmission distance of 3×10^6 km in the Taiji, m_{flat} is as large as 2.5×10^4. The bigger the m_{flat}, the closer the laser beam is to a flat top beam. However, with restricted distance in the on-ground experiment, we can only increase m_{flat} by adjusting the value of ω_0 as well as reducing the aperture size. Thus, as introduced in section 2.1, we replace the telescope by a small aperture.

From Table I, it can also be found that the radius of the uncertainty cone R_{uc} is larger than the receiving beam size. As a result, a scanning strategy must be carried out for ensuring successful acquisition. In order to simulate the scanning process, we define the scanning range coefficient n_{scan} as the ratio of R_{uc} and ω_z. After expansion, n_{scan} is given by,

$$n_{scan} = \frac{\alpha}{\sqrt{\frac{\omega_0^2}{L^2} + \frac{\lambda^2}{\pi^2 \omega_0^2}}}, \tag{2}$$

where, α is the half angle of scanning range. n_{scan} also increases with the increase of L. Thus, with particular α and ω_0, the simulation of n_{scan} is also limited to the beam propagation distance on-ground.

The receiving laser power can be estimated by [22],

$$P_{rec} = \frac{\pi^2 \varepsilon^4}{\lambda^2 L^2} \tau P_{out}, \tag{3}$$

where, λ is the wavelength, τ is the transmittance in space and P_{out} is the outgoing laser power at the transmitting telescope. For the Taiji program, P_{out} is approximate 1 W. Assuming $\tau = 1$, P_{rec} can be estimated as 1.5 nW. As less than 10% of the receiving laser power will be allocated to the acquisition camera, the laser power received by the CMOS is only 100 pW magnitude.

From formula (1)-(3), it can be found that there is strong coupling in the design of system parameters. For instance, change trend of m_{flat} and n_{scan} with respect to ω_0 is contrary, while the value of ε influences m_{flat} as well as P_{rec}. Thus, flat top beam, scanning range and receiving laser power simulation should be comprehensively considered. The right column of Table. I presents the system parameters used in the experiment. Although P_{rec} reaches 1 μW magnitude with $P_{out} = 1$ mW and $L = 10$ m, the laser power received by CMOS can be attenuated to 100 pW magnitude with attenuators. As a lens, whose focal length $f = 150$ mm, is used to image the laser beam, the laser spot on the CMOS is an Airy spot. Assuming the pixel size of r_n, the spot size expressed by pixel number can be estimated as,

$$r = 0.61 \frac{\lambda f}{\varepsilon r_n}. \tag{4}$$

Thus, the photo-electron number of the spot center pixel can be written as,

$$n_{center} = \frac{\int_{-3.83/r}^{3.83/r} (2J_1(\psi)/\psi)^2 d\psi}{\int_{-3.83}^{3.83} (2J_1(\psi)/\psi)^2 d\psi} \cdot n_o, \tag{5}$$

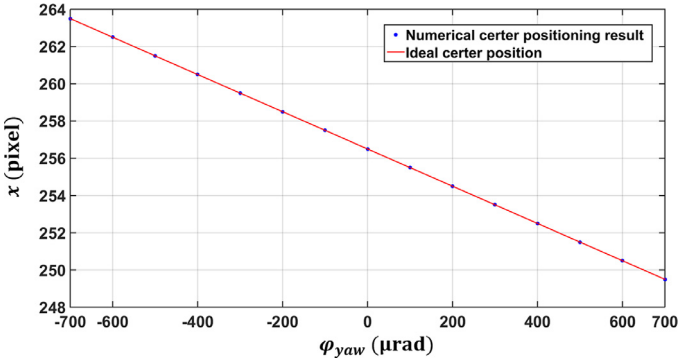

Fig. 2. Comparison between numerical spot center positioning result and the ideal spot center position.

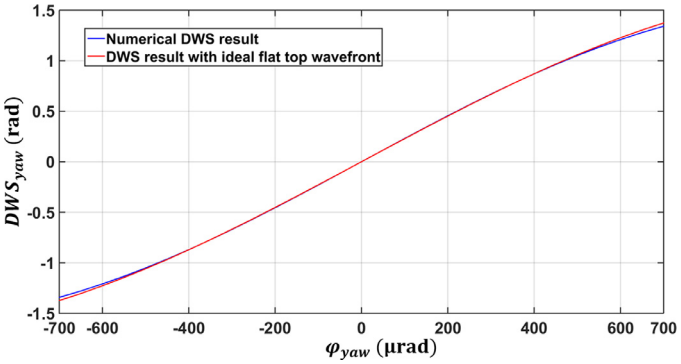

Fig. 3. Comparison between numerical DWS result and the DWS result with ideal flat top wavefront.

$$n_o = \frac{P_0 \lambda}{hc}\eta, \tag{6}$$

where, n_o is the total photo-electron number, $J_1(\psi)$ is the Bessel function of ψ, h is the Planck constant and η is the conversion efficiency. Thus, with $\varepsilon = 0.5$ mm, $r_n = 15$ μm/pixel, $P_0 = 100$ pW and $\eta = 0.7$, n_{center} is estimated as about 3×10^6 e^-. The CMOS we used in the experiment is Tekwin SH640, whose mean value of noise electrons is 1.5×10^5 e^-/pixel. Therefore, around the spot center, the photo-electron number is far larger than the noise electron number and the detector has enough signal to noise ratio (SNR) for detecting weak light based on improved centroid method [7]. As the NEP(Noise Equivalent Power) of the QPD in the experiment is not small enough, the interference signal is generated by a local beam of 10 μW magnitude and a receiving beam of 100 nW magnitude.

Because of limited angular dynamic range of the hexapod, the value of n_{scan} can hardly be restored. As a result, the optical platform acquires the receiving light easily with simple scan. To fully verify the scanning process with small n_{scan} and increase signal to noise ratio, a threshold is set for the receiving laser spot on CMOS. The scanning process will continue until the maximum detected grey value of the CMOS exceeds the threshold.

We can approximately simulate a flat top beam with the m_{flat} of 13. However, as the value of m_{flat} in the experiment is far less than that in the actual system, influence of in-flat top properties to the target precision should be carefully considered. In the acquisition phase, laser spot center is positioned based on the centroid method. However, if the intensity distribution is in-homogeneity within the aperture area, the laser spot center position deviates from its centroid position. As a result, the acquisition precision decreases. For estimating the effect, numerical method is used. Firstly, the experimental optical system is simulated using ASAP software. With different beam incident directions, the intensity distribution on the CMOS camera is recorded. Then, we use the centroid method to obtain the laser spot center position based on Matlab platform. The numerical results are shown in Fig. 2 as the blue spot, while results of the red line correspond to the exact value with flat top beam incidence.

It can be seen that the numerical results well coincide with the ideal center position. The in-flat top property also affects the DWS measurement, as the beam transmitting direction is inconsistent within the aperture area. To analyse the influence, the same numerical method is carried out. The results in Fig. 3 illustrate that the DWS technique works well and the maximum measurement error induced by in-flat top properties is smaller than the required precision. Therefore, the in-flat top properties can be ignored with the designed parameters.

3. Experiment

As illustrated in Fig. 4(a), we constructed the experimental system based on the diagram in Fig. 1. Two optical platforms are placed at each end of a marble vibration isolation platform, with the details shown in Fig. 4(b). The optical platforms are respectively set up on hexapods, while the hexapods are installed on four-axis manual displacement stages. As the angular dynamic range of the hexapod is only ±700 μrad, manual displacement stages are used for initial pointing and making the half angle of the uncertainty cone smaller than 700 μrad. The whole system is protected by glass cover to lower the impact of air turbulence and temperature fluctuation to interference measurement.

Before the experiment, we firstly calibrate the reference position of the CMOS camera. The pitch and yaw direction of the hexapod are adjusted until the DWS signal of each direction equals to zero. At this time, the laser spot position on the CMOS is defined as the reference position. Then, we calibrate the angle-position conversion coefficient of CMOS and angle-phase conversion coefficient of DWS respectively by fitting the angular displacement with respect to measurement results of spot center positioning and DWS technique.

For examining the measurement capability of the experimental system, we test the background noise level, which is estimated by the root mean square (RMS) value in acquisition phase and the amplitude spectral density (ASD) within the frequency band of 1 mHz - 1 Hz in laser pointing phase. Only the results in the yaw direction is introduced, as the same conclusion can be obtained in the pitch direction. Without any control, Fig. 5 presents the continuous results of laser spot center positioning. The RMS value is calculated as $x_{rms} = 0.0073$ pixel, corresponding to $\varphi_{x,rms} = 0.73$ μrad. The center positioning error is mainly generated by background noise of the CMOS and the quantization noise of the centroid method. As the acquisition precision is read out by the DWS signal, its performance should also be considered. Fig. 6 shows the angular measurement results produced by the DWS technique in both time and frequency domain. With the results in the time domain, we can obtain the DWS read out precision as $\varphi_{yaw,rms} = 0.24$ μrad. Thus, the background read out noise in the acquisition phase is $\sqrt{\varphi_{x,rms}^2 + \varphi_{yaw,rms}^2} = 0.77$ μrad, far smaller than the requirement of 400 μrad. The results in the frequency domain show that the maximum value of $\varphi_{yaw,ASD}$ is smaller than the requirement of 4 μrad/$\sqrt{\text{Hz}}$. Therefore, the experimental system has the potential to fulfill the precision requirement of the Taiji in both acquisition phase and laser pointing phase.

For fully simulating the whole laser link acquisition process, the experiment is divided into four successive stages.

(1) Stage I: Initialization. After initializing of each device, the optical platforms arbitrary adjust their attitude within the uncertainty cone and wait for the start command of acquisition.

Fig. 4. (a) Physical picture of the laser link construction on-ground experimental system. (b) Physical picture of the optical platform. Two identical optical platforms are placed at each end of the marble vibration isolation platform.

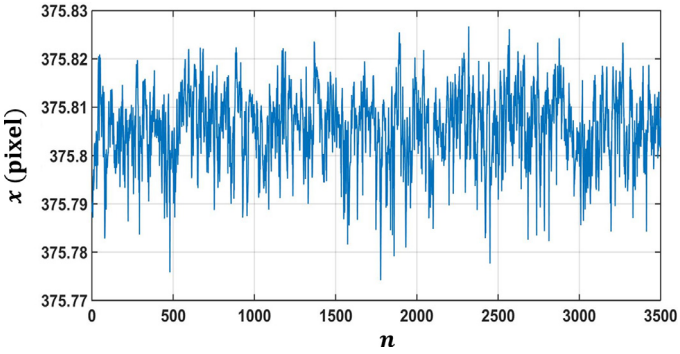

Fig. 5. The continuous results of laser spot center positioning in the x-direction of the CMOS without any control. The RMS value of the data is $x_{rms} = 0.0073$ pixel.

(2) Stage II: Coarse acquisition. At first, for covering the whole uncertainty cone of $P2$, $P1$ platform performs Archimedes spiral scanning, which is denoted as,

$$\vec{r} = \frac{d}{2\pi}\phi(t)\begin{pmatrix} cos\phi(t) \\ sin\phi(t) \end{pmatrix}, where\ \phi(t) = 2\pi\frac{r_{max}}{d}\sqrt{\frac{t}{T}}. \quad (7)$$

Here, d is the arc separation, T is the total scanning time and r_{max} is the maximum value of the spiral radius. Meanwhile, $P2$ platform is used as the laser receiving terminal and stares into its initial direction. At a certain time, $P2$ receives the laser signal with enough power on its CMOS camera. Based on the laser center positioning result, the line of sight direction of $P2$ is adjusted for pointing to $P1$. At this time, the CMOS on $P1$ can also receive enough laser power. With the same method, $P1$ can change its attitude and point to $P2$. As the laser beam has to transmit about 10 s between the satellites in the Taiji program, the scanning satellite will keep scanning until it receive enough laser power. For simulating the process, we introduce a certain delay during the scanning.

(3) Stage III: Fine acquisition. After course acquisition, the two platforms point to each other. Then, feedback close loop control is carried out based on the CMOS read out. For the Taiji program, frequency scanning is performed during this stage for obtaining the interference signal on the QPDs. Thus, in the experiment, a certain delay is introduced for simulating the process as well as examining the acquisition precision.

(4) Stage IV: Laser pointing. Finally, the hexapod control is based on the DWS signal rather than CMOS signal in this stage. The laser pointing precision is estimated by the ASD of the DWS read out.

4. Results and Discussion

The laser link construction simulation can be automatically fulfilled with our self-developed upper computer software based on C$_{++}$. As the maximum initial angular deviation is approximate 700 μrad (within the linearity range of the DWS), the whole process can be read out by the DWS technique. One of the whole process record based on the current setup is shown in Fig. 7. Similarly, only the results in the yaw direction is presented. It can be seen that the initial angular deviation of $P1$ and $P2$ are approximately −270 μrad and 500 μrad respectively.

In stage II, $P1$ performs Archimedes spiral scanning. Its projection on the yaw direction is like a sinusoidal wave, whose amplitude is increasing. At the end of this stage, both platforms point to each other with single open loop control. After that, feedback close loop control is carried out for fine acquisition with details shown in Fig. 8. The acquisition precision at the QPD is estimated by the mean value of the DWS readout data as $\varphi_{1,mean} = -8.94$ μrad, $\varphi_{2,mean} = 8.29$ μrad. As introduced in section 2.1, the corresponding acquisition requirement at the QPD is 400 μrad. Thus, it can be concluded that we achieve the acquisition precision more than an order of magnitude smaller than the requirement. We have known from section 3 that the background readout noise is about 1 μrad in acquisition phase. Except for that, the acquisition precision may deteriorate because of reference position deviation generated by calibration error and displacement stage long-term drift. Thus, the acquisition precision can further improve by increasing system readout precision and change the manual displacement stage to a stable electric displacement stage.

Based on the data in the laser pointing stage, we obtain the ASD of angular measurement results, as illustrated in Fig. 9. We can conclude that the laser pointing precision is smaller than the requirement of 4 μrad/$\sqrt{\text{Hz}}$. By comparing with the result in Fig. 6, it can be also found that the laser pointing precision is close to the background noise level. Thus, background noise is the main noise source in this stage. As

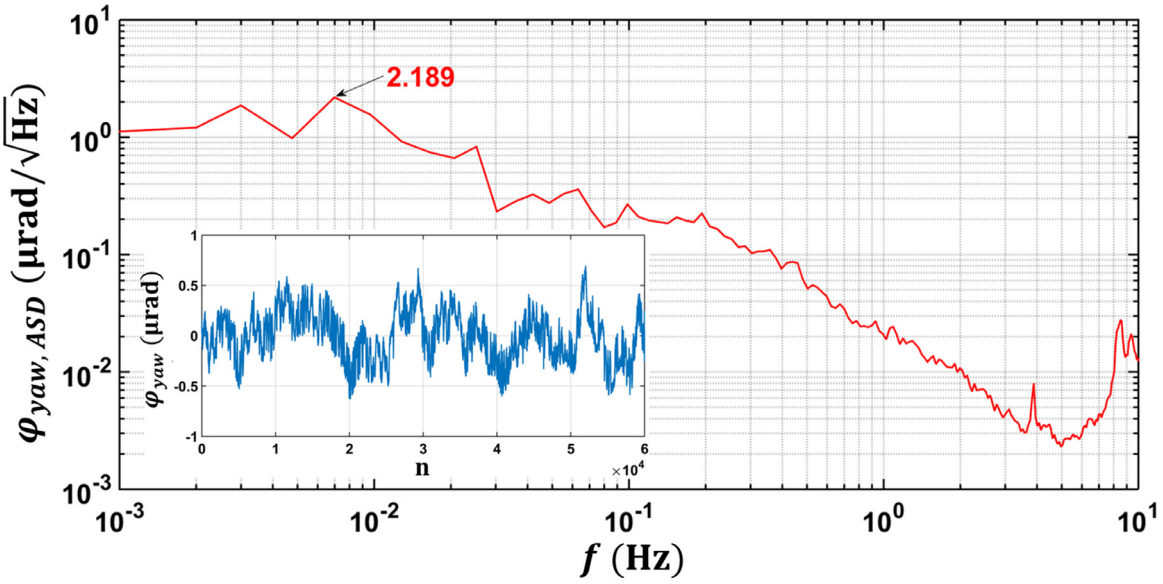

Fig. 6. The background angular measurement results produced by the DWS technique in the yaw direction. Where, the blue line is the results in the time domain and the red line is the ASD results in the frequency domain. The RMS of the data is $\varphi_{yaw,rms} = 0.24$ μrad and the maximum value of the ASD data is 2.189 μrad/$\sqrt{\text{Hz}}$

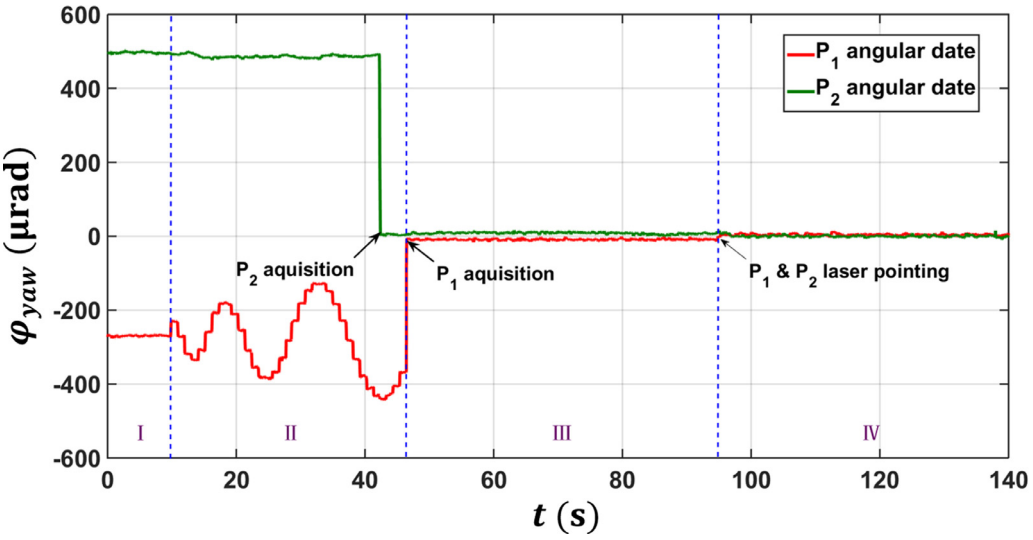

Fig. 7. Whole process experimental result of laser link construction in the yaw direction. The whole process is divided into four stages: initialization, coarse acquisition, fine acquisition and laser pointing. Where, the red line is the angular data of the $P1$ platform and the green line is the angular data of the $P2$ platform.

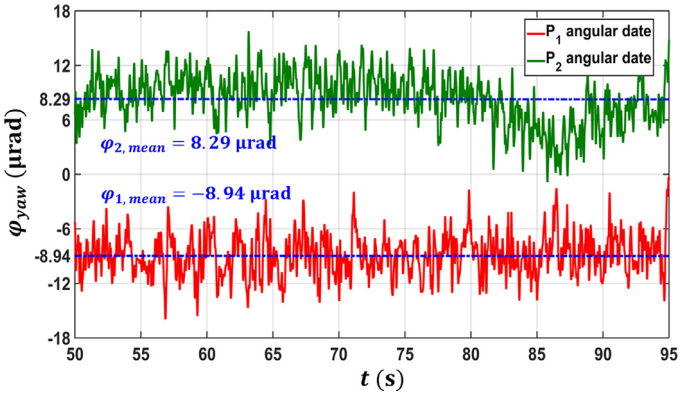

Fig. 8. Fine acquisition results. Where, the red line and the green line are respectively the angular data of $P1$ and $P2$. The mean value of the results $\varphi_{1,mean} = -8.94$ μrad, $\varphi_{2,mean} = 8.29$ μrad are regarded as the acquisition precision.

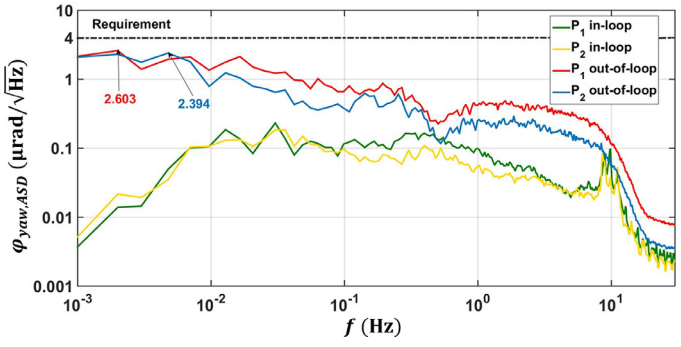

Fig. 9. Laser pointing results. Where, the red line and the blue line are the ASD results of $P1$ and $P2$ out-of-loop data respectively, the green line and the yellow line are the ASD results of $P1$ and $P2$ in-loop data respectively. The black dash dot is the requirement of the Taiji program.

the experimental system exposes in the atmospheric environment, the background noise mainly comes from the air turbulence and temperature fluctuation. For further reducing the noise level, the experiment has to be carried out in a vacuum chamber. Anyhow, the precision requirement in both acquisition and laser pointing phase can be fulfilled with the current set up.

5. Summary

Aiming at establishing a stable inter-satellite laser interferometer, LISA-like gravitational wave detection missions need to construct a 10^6 km laser link with the pointing jitter suppressed to 10 $\mathrm{nrad}/\sqrt{\mathrm{Hz}}$. Thus, a dedicated laser acquisition and pointing scheme with three different detectors is proposed for the extremely tough task. The purpose of the current study was to fully verify the feasibility of the proposed scheme and resolve the relevant technique problems based on experimental method. We comprehensively considered the simulation of actual optical system, acquisition & pointing process, far field beam receiving characteristics as well as target accuracy and designed the optical system as well as the system parameters. Because of restricted beam transmitting distance and limited angular dynamic range of the hexapod, most parts can be well restored in the experiment except for the simulation of flat top beam and scanning range. The numerical results show that the influence of in-flat top properties to the acquisition and pointing precision is smaller than the requirement with the designed parameters. Based on the design, we established the laser link construction experimental system. The whole laser acquisition and pointing process can be carried out automatically. The results present that the achieved laser acquisition precision is more than an order of magnitude smaller than the requirement, while the laser pointing precision can also fulfill the requirement.

The present study appears to be the first study to experimentally demonstrate the proposed laser link construction scheme. The laser acquisition and pointing precision requirement can be achieved in the case of actual working condition simulation. For further improving the precision, the experiment has to be carried out under the vacuum condition. The results show clearly that the three-stages detector scheme is feasible in the space-based gravitational wave detection mission. The design methods of the experimental system have the potential to be used in other space applications.

Funding

The authors would like to thank the National Key R&D Program of China (2020YFC2200104), and the Strategic Priority Research Program of the Chinese Academy of Sciences for the financial support (Project No. XDA1502110102, No. XDA1502110103)

Declaration of Competing Interest

The authors declare that they have no known competing financial interests or personal relationships that could have appeared to influence the work reported in this paper.

CRediT authorship contribution statement

Ruihong Gao: Conceptualization, Methodology, Formal analysis, Investigation, Writing – original draft. **Yikun Wang:** Investigation, Data curation, Visualization, Writing – review & editing. **Zhao Cui:** Investigation, Software, Data curation. **Heshan Liu:** Software, Formal analysis. **Anwei Liu:** Validation. **Xingguang Qian:** Software. **Xue Wang:** Software. **Zhixiong Yao:** Validation. **Qiujie Yang:** Validation. **Jianjun Jia:** Funding acquisition. **Keqi Qi:** Validation. **Shaoxin Wang:** Validation. **Ziren Luo:** Conceptualization, Methodology, Supervision, Writing – review & editing. **Gang Jin:** Supervision, Writing – review & editing. **Jianyu Wang:** Formal analysis, Project administration.

References

[1] Cirillo F. Controller design for the acquisition phase of the LISA mission using a kalman filter. University of Pisa; 2007. Ph.D. thesis.
[2] Cirillo F, Gath PF. Control system design for the constellation acquisition phase of the LISA mission. Journal of Physics: Conference Series 2009;154. doi:10.1088/1742-6596/154/1/012014.
[3] Dong Y, Liu H, Luo Z, Li Y, Jin G. Methodological demonstration of laser beam pointing control for space gravitational wave detection missions. Review of Scientific Instruments 2014;85. doi:10.1063/1.4891037.
[4] Duan H, Liang Y, Yeh H. Analysis of non-linearity in differential wavefront sensing technique. Optics Letters 2016;41. doi:10.1364/OL.41.000914.
[5] Gath PF, Schulte HR, Weise D, Johann U. Drag free and attitude control system design for the LISA science mode. AIAA Guidance, Navigation and Control Conference and Exhibit 2007.
[6] Gao R, Liu H, Luo Z, Jin G. Introduction of taiji program laser pointing scheme. Chinese Optics 2019;3. doi:10.3788/CO.20191203.0425.
[7] Gao R, Liu H, Zhao Y, Luo Z, Jin G. High-precision laser spot center positioning method for weak light conditions. Applied Optics 2020;59. doi:10.1364/AO.381626.
[8] Gerberding O. Phase readout for satellite interferometry; 2014. Ph.D. thesis.
[9] Hechenblaikner G. Measurement of the absolute wavefront curvature radius in a heterodyne interferometer. Journal of the Optical Society of America A 2010;27. doi:10.1364/JOSAA.27.002078.
[10] Henein S, Spanoudakis P, Schwab P, et al. Design and development of the point-ahead angle mechanism for the laser interferometer space antenna (lisa). 13th European Space Mechanisms and Tribology Symposium ESMATS 2009 2009.
[11] Hyde TT, Maghami PG, Merkowitz SM. Pointing acquisition and performance for the laser interferometry space antenna mission. CLASSICAL AND QUANTUM GRAVITY 2004;21. doi:10.1088/0264-9381/21/5/036.
[12] Isleif K-S, Heinzel G, Mehmet M, Gerberding O. Compact multifringe interferometry with subpicometer precision. Physical Review Applied 2019;12. doi:10.1103/PhysRevApplied.12.034025.
[13] Jennrich O, Binetruy P, Stebbins R, et al. Ngo revealing a hidden universe: opening a new chapter of discovery Assessment Study Report. European Space Agency; 2011.
[14] Jono T, Takayama Y, Kura N, et al. Oicets on-orbit laser communication experiments. Free-Space Laser Communication Technologies XVIII 2006;6105. doi:10.1117/12.673751.
[15] Liao S, Cai W, et al. Satellite-to-ground quantum key distribution. Nature 2017;549:43–7. doi:10.1038/nature23655.
[16] Luo Z, Wang Y, Wu Y, et al. The taiji program: A concise overview. Progress of Theoretical and Experimental Physics 2020. doi:10.1093/ptep/ptaa083.
[17] Maghami PG, Hyde TT, Kim J. An acquisition control for the laser interferometer space antenna. CLASSICAL AND QUANTUM GRAVITY 2004;22. doi:10.1088/0264-9381/22/10/038.
[18] Mahrdt C. Laser link acquisition for the GRACE follow-on laser ranging interferometer. Gottfried Wilhelm Leibniz Universit Hannover; 2014. Ph.D. thesis.
[19] Morrison E, Meers BJ, Robertson D, Ward H. Experimental demonstration of an automatic alignment system for optical interferometers. Applied Optics 1994;33. doi:10.1364/AO.33.005037.
[20] Morrison E, Meers BJ, Robertson D, Ward H. Automatic alignment of optical interferometers. Applied Optics 1994;33. doi:10.1364/AO.33.005041.
[21] Sanjuan J, Gohlke M, et al. Interspacecraft link simulator for the laser ranging interferometer onboard GRACE follow-on. Applied Optics 2015;54:6682–9. doi:10.1364/AO.54.006682.
[22] Steier F. Interferometry techniques for space-borne gravitational wave detectors. Gottfried Wilhelm Leibniz Universitt Hannover; 2014. Ph.D. thesis.
[23] Tolker-Nielsen T, Oppenhauser G. In-orbit test result of an operational optical intersatellite link between ARTEMIS and SPOT4, SILEX. Free-Space Laser Communication Technologies XIV 2002;4635. doi:10.1117/12.464105.
[24] Tolker-Nielsen T. Pointing, acquisition and tracking system for the free space laser communication system, SILEX. Free-Space Laser Communication Technologies VII 1995;2381. doi:10.1117/12.207403.
[25] Wu C. Study of inter-satellites laser communication terminals and its laboratory testing platforms optical system. Changchun Institute of Optics, Fine Mechanics and Physics Chinese Academy of Sciences; 2014. Ph.D. thesis.